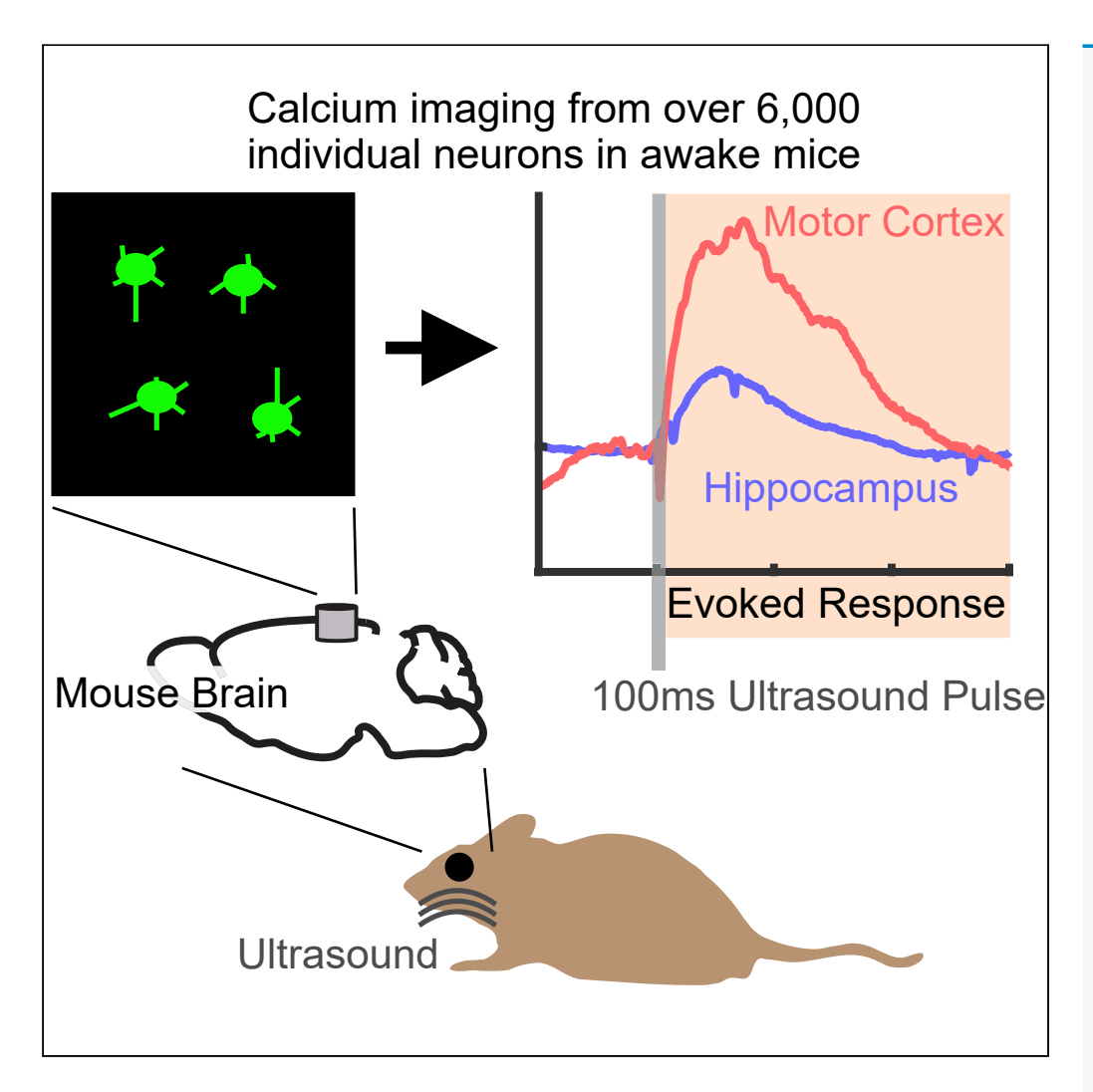
iScience



Article

Region-specific effects of ultrasound on individual neurons in the awake mammalian brain



Hua-an Tseng, Jack Sherman, Emma Bortz, ..., Dana Zemel, Thomas Szabo, Xue Han

xuehan@bu.edu

Highlights

Ultrasound increases intracellular calcium in individual neurons in awake mice

Hippocampal CA1 responds to ultrasound with a latency shorter than 50 ms

Ultrasound evoked response in CA1 is shorter and smaller than the motor cortex

Ultrasound-evoked responses are brain region specific

Tseng et al., iScience 24, 102955 September 24, 2021 © 2021 The Authors. https://doi.org/10.1016/ j.isci.2021.102955



iScience



Article

Region-specific effects of ultrasound on individual neurons in the awake mammalian brain

Hua-an Tseng,¹ Jack Sherman,^{1,2} Emma Bortz,¹ Ali Mohammed,¹ Howard J. Gritton,^{1,3} Seth Bensussen,¹ Rockwell P. Tang,¹ Dana Zemel,¹ Thomas Szabo,¹ and Xue Han^{1,4,*}

SUMMARY

Ultrasound modulates brain activity. However, it remains unclear how ultrasound affects individual neurons in the brain, where neural circuit architecture is intact and different brain regions exhibit distinct tissue properties. Using a high-resolution calcium imaging technique, we characterized the effect of ultrasound stimulation on thousands of individual neurons in the hippocampus and the motor cortex of awake mice. We found that brief 100-ms-long ultrasound pulses increase intracellular calcium in a large fraction of individual neurons in both brain regions. Ultrasound-evoked calcium response in hippocampal neurons exhibits a rapid onset with a latency shorter than 50 ms. The evoked response in the hippocampus is shorter in duration and smaller in magnitude than that in the motor cortex. These results demonstrate that noninvasive ultrasound stimulation transiently increases intracellular calcium in individual neurons in awake mice, and the evoked response profiles are brain region specific.

INTRODUCTION

Ultrasound represents a promising technique for targeted noninvasive neuromodulation because of its unique tissue-penetrating properties (King et al., 2013; Tufail et al., 2010; Ye et al., 2016; Tyler, 2012). Ultrasound, acoustic waves of over 20kHz, was first reported to modulate nerves and muscles back in the 1920s (Harvey, 1929). Over the past century, a number of in vivo studies have demonstrated that a wide range of ultrasound frequencies delivered via a broad set of pulse protocols can stimulate peripheral nerves, the spinal cord, and the brain with varying efficiency (Tufail et al., 2011). In Caenorhabditis elegans, ultrasound was shown to elicit motor behavioral responses through activating specific mechanosensitive channels (Kubanek et al., 2018). In rodents, several studies demonstrated that ultrasound directed to the motor cortex can successfully elicit muscle responses (Li et al., 2016; Lee et al., 2018; King et al., 2013). In humans and nonhuman primates, ultrasound can effectively stimulate somatosensory receptors in the hand and modulate responses in the somatosensory cortex and other brain regions (Gavrilov et al., 1976; Legon et al., 2012, 2014; Lee et al., 2015, 2016; Yang et al., 2018, 2021; Kim et al., 2017; Yuan et al., 2020). These studies, though providing convincing evidence that ultrasound can modulate neural activity in intact brain circuits, rely largely on recording downstream motor activations via electromyography (EMG) or aggregated neural signals, such as electroencephalogram (EEG), functional magnetic resonance imaging (fMRI), and functional near-infrared spectroscopy (fNIR), which are either indirect measures of neural activity or have poor spatiotemporal resolution. So far, it remains unknown how individual neurons are modulated by ultrasound stimulation in the living brain.

Ultrasound generates nonthermal neuromodulation effects (Ter Haar, 2007; Tufail et al., 2010; Menz et al., 2013) through a number of mechanical interactions with targeted cells, such as activating mechanosensitive channels or producing membrane deformation, all of which can alter membrane conductance and thus neuronal excitability (Kubanek et al., 2016; Fini and Tyler, 2017; Krasovitski et al., 2011; Plaksin et al., 2016; Tyler, 2012; Dinno et al., 1989; Velling and Shklyaruk, 1988). Many *in vitro* studies have provided convincing evidence on the involvement of several types of mechanosensitive channels in mediating ultrasound stimulation effects in neurons through altering plasma membrane conductance. Altered membrane conductance, however, can excite or inhibit neurons, depending on the specific biophysical properties of the stimulated neurons, and the spatiotemporal profiles of the evoked conductance vary depending on the



¹Biomedical Engineering Department, Boston University, Boston, MA 02215, USA

²Department of Pharmacology and Experimental Therapeutics, Boston University, Boston, MA 02215, USA

³Department of Comparative Biosciences at the University of Illinois at Urbana Champaign, Urbana, IL 61802, USA

⁴Lead contact

^{*}Correspondence: xuehan@bu.edu

https://doi.org/10.1016/j.isci. 2021.102955





specific ultrasound stimulation parameters (Fry et al., 1958; Tyler et al., 2008; Lin et al., 2019). Indeed, recent observation that the same set of ultrasound stimulation protocol can evoke both excitatory and inhibitory effects in the somatosensory circuits depending on sensory stimulation states underscores the need of high resolution, single neuron level analysis of ultrasound effects in the brain with intact neural circuits (Yang et al., 2021).

In addition to neurons, there are about ten-fold more astrocytes in the brain that are also responsive to mechanical stimulation. Recently, using calcium imaging, Oh et al. demonstrated that ultrasound activates astrocytes in the mouse brain through recruiting mechanosensitive channels, suggesting that ultrasound can modulate intracellular calcium concentrations without the involvement of action potentials (Oh et al., 2020). Ultrasound-mediated astrocyte activation in turn could alter surrounding neurons' activity through astrocytic release of neurotransmitter glutamate (Yang et al., 2015). Additionally, ultrasound can produce varying mechanical forces at distinct tissue interfaces depending on the magnitude of tissue acoustic impedance mismatch (Tyler, 2012), leading to potentially different ultrasound response thresholds for different brain regions. Recent studies in anesthetized mice and guinea pigs demonstrated that cochlear fluid when vibrated by ultrasound could also activate auditory pathways, highlighting the importance of considering tissue architectures and cranial bone structures when studying ultrasound effects in the intact brain (Sato et al., 2018; Guo et al., 2018). Finally, in a living brain, different brain regions not only contain a wide variety of neuron subtypes with varying mechanosensitive protein expressions and membrane biophysical properties, but also have heterogeneous synaptic connectivity patterns and tissue structures. However, it is unknown whether ultrasound produces distinct effects in different brain regions.

To quantify how individual neurons in different brain regions respond to ultrasound stimulation, we performed large-scale calcium imaging using genetically encoded calcium sensor GCaMP6 in awake head-fixed mice. We demonstrate that brief 100-ms-long pulses of ultrasound reliably elicit transient increases in intracellular calcium concentration in a large fraction of individual neurons in both the hippocampus and the motor cortex. Hippocampal neurons can be rapidly modulated by ultrasound with a latency of less than 50 ms, faster than the temporal resolution of our calcium imaging measurement technique. Additionally, hippocampal responses are shorter in duration and smaller in magnitude comparing to motor cortex responses. Our computational simulation results indicated that the maximum instantaneous pressure in the motor cortex was only 8.2% more than that in the hippocampus during the 100-ms-long stimulation period, which cannot directly account for the over two-fold difference in the evoked response amplitude observed between the two brain regions, and the several-second-long variations in evoked response duration. Together, these findings provide direct evidence that noninvasive ultrasound stimulation activates individual neurons through elevating intracellular calcium concentration in multiple brain regions in awake rodents free of anesthesia effects, and ultrasound-evoked responses are transient and brain region specific.

RESULTS

Individual hippocampal CA1 neurons are activated by 100-ms-long pulsed ultrasound stimulation

To examine the effects of ultrasound stimulation in the brain with single-neuron resolution, we performed GCaMP6 calcium imaging in awake head-fixed mice (Figure 1A). AAV-Syn-GCaMP6f virus was injected into the hippocampus CA1 region to selectively label neurons using the synapsin promoter, and an imaging window was surgically implanted over the CA1 to allow for optical access (Figure 1B). Calcium imaging was performed with a custom wide-field microscope at an acquisition rate of 20 Hz, while mice were awake and stimulated with a planer ultrasound transducer placed underneath the head (Figure 1A). During each imaging session, mice experienced 20 trials of ultrasound stimulations, with each trail lasting 30 or 60 s. Ultrasound stimulation occurred 10 s after the onset of calcium imaging data acquisition in each trail. Each stimulation consisted of 200 pulses at 2 kHz, with each pulse containing 75 cycles of 350 kHz sine wave ultrasound delivered at ~0.44 MPa peak pressure, similar to that used in Tufail et al. (Tufail et al., 2011). To estimate the distribution of ultrasound intensity in the brain with our experimental configurations, we simulated the ultrasound wavefield using k-wave acoustic toolbox in MATLAB following the framework of Mueller et al., 2007). Mouse skulls were formed from the three-dimensional digital atlas (Chan et al., 2007) and modified to include the specific designs of the imaging chambers used here. Our simulation results indicated that the hippocampus area under the imaging window received a maximum



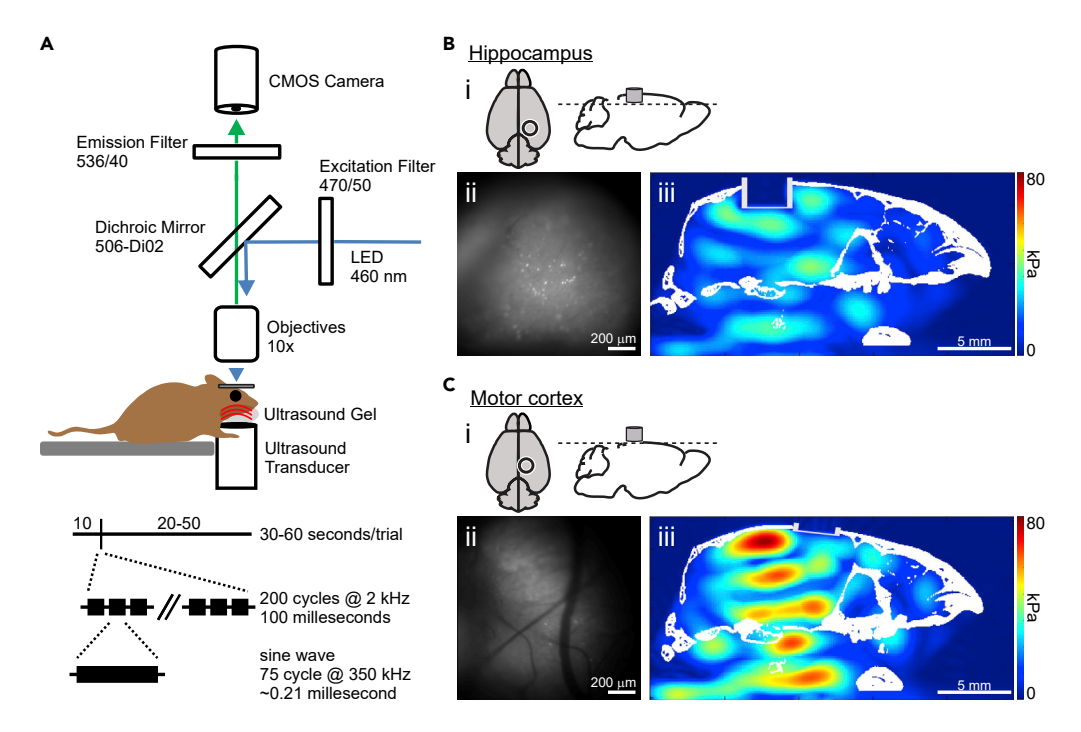


Figure 1. Experimental setup and protocols for simultaneous in vivo calcium imaging and ultrasound stimulation

(A) Illustration of an animal head-fixed through a surgically installed head fixation bar, over a stationary platform. A conventional planar ultrasound transducer was placed under animal's head, and ultrasound gel was used to fill the gap between the ultrasound transducer and the animal's head. GCaMP6 was excited with a 460nm LED and fluorescence signals were collected with a 10x objective lens and an sCMOS camera at 20 Hz through a surgically implanted imaging window. Each imaging session consisted of 20 trials, 30–60 s long. Each trial included a 10 s baseline period, and a 20–50 s post stimulation period. Ultrasound stimulation contained 75 cycles of 350 kHz ultrasound in a pattern of 200 cycle at 2 kHz.

(B) Illustration of the experimental configuration used to analyze ultrasound effect in the hippocampus. (Bi) Configuration of calcium imaging window placement over the hippocampus, top view (left) and sagittal view (right). (Bii) A projection image from an example calcium imaging experiment. (Biii) Computational simulation of ultrasound pressure distribution in the brain. Skull and imaging chamber were highlighted in white.

(C) Similar to (B), but for experimental configuration used to test ultrasound effects in the motor cortex.

instantaneous pressure of 24.3 kPa (Figure 1B), whereas the motor cortex area under the imaging window received 26.3 kPa (Figure 1C).

To quantify ultrasound-evoked responses in CA1 neurons, we motion corrected the recorded calcium imaging videos, segmented individual neurons, extracted GCaMP6 fluorescence trace for each neuron, and then normalized each GCaMP6 fluorescence trace to the corresponding mean fluorescence intensity during the 10-s period before ultrasound onset. Upon ultrasound stimulation, many CA1 neurons exhibited a rapid increase in GCaMP6 fluorescence immediately after ultrasound onset (Figures 2A and 2B), and the fluorescence intensity peaked within a couple of seconds, and then diminished after about 5–10 s. To determine whether a neuron is activated by ultrasound stimulation, we compared the averaged GCaMP6 fluorescence intensity within the response period (5-s window after ultrasound onset) to the baseline period (5-s window immediately before ultrasound onset) across all 20 trials, using a Wilcoxon rank-sum test with a threshold of p < 0.05. We found that 1067 of the 5868 recorded neurons (18.2%) were significantly activated, exhibiting increased GCaMP6 fluorescence intensity upon ultrasound stimulation (Figure 2F and Table 1, n = 5868 neurons from 23 imaging sessions in 14 mice). We further validated that the Wilcoxon rank-sum test statistical method used to identify activated individual neurons was sufficiently powered using a bootstrapping analysis (Details see STAR Methods), confirming that our statistical tests yielded a false positive rate of $\sim 0.02\%$.



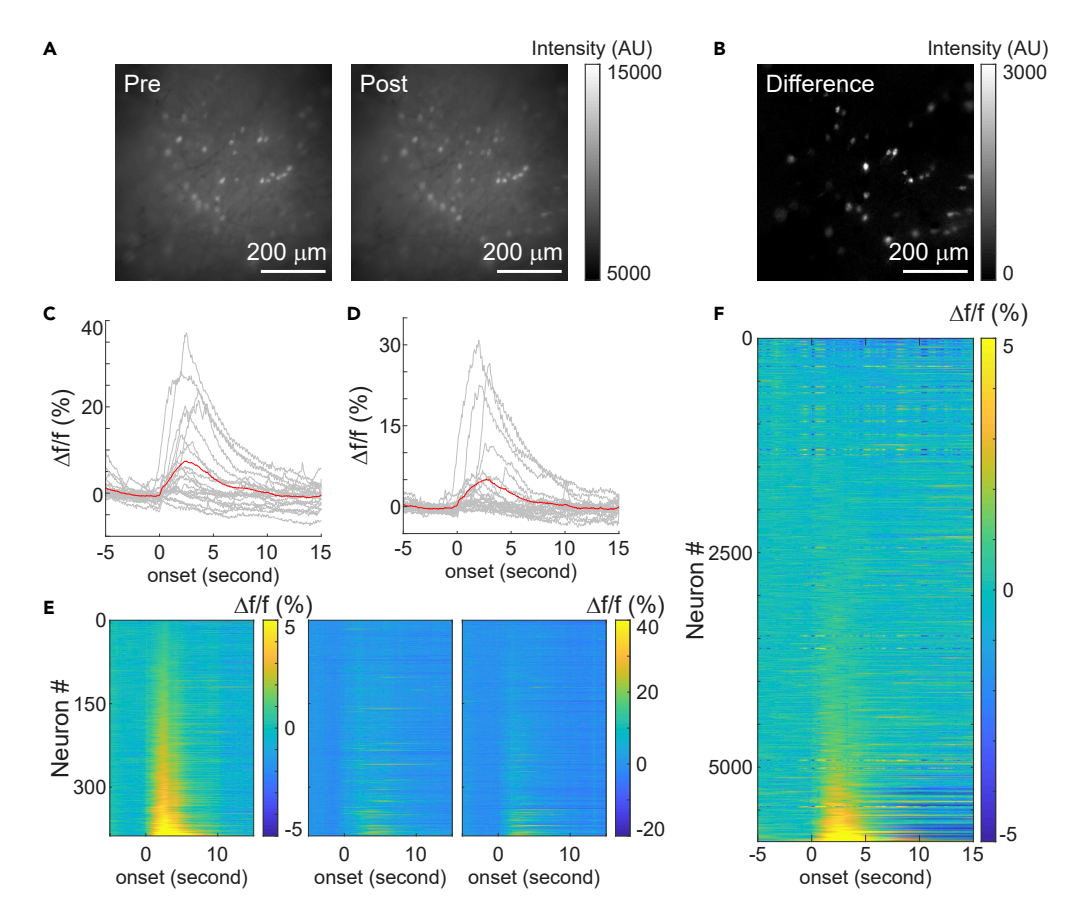


Figure 2. Individual hippocampal neurons are activated by pulsed ultrasound stimulation

(A) Example GCaMP6 fluorescence from one field of view containing hundreds of individual neurons before (left, max fluorescence intensity projection of 5-s imaging period before ultrasound onset) and after ultrasound stimulation onset (right, max intensity projection of 5-s imaging period after ultrasound onset). The images shown are 25% of the total field of view.

- (B) The difference of GCaMP6 fluorescence intensity before and after stimulation onset. The bright spots indicate neurons with elevated GCaMP6 fluorescence induced by ultrasound.
- (C and D) GCaMP6 signals from two example neurons aligned to the ultrasound onset. Gray lines are individual trial responses (n = 20 trials), and the red line is the averaged response across all 20 trials.
- (E) Trial averaged GCaMP6 signals (n = 20 trials), and two example individual trial responses (middle and right) from simultaneously recorded individual neurons in the same field of view (left), sorted based on the trial averaged fluorescence intensity during the 5-s window after ultrasound onset.
- (F) Trial-averaged response from all 5868 recorded neurons, sorted by intensity during the 5-s window after ultrasound onset. Each line represents the averaged GCaMP6 fluorescence intensity of an individual neuron across 20 trials of ultrasound stimulation.

We noted some variations in individual neuron response to ultrasound stimulation on a trial-by-trial basis, but activated neurons in general exhibited increase in GCaMP6 fluorescence across trials (Figures 2C and 2D). To visualize the variation of ultrasound effect across trials, we sorted simultaneously recorded neurons by their trial-averaged intensity during the response period across all 20 trials (Figure 2E, left) and plotted their corresponding GCaMP6 signals during individual trials (Figure 2E, middle and right). We found that ultrasound stimulation activated slightly different subsets of neurons in each trail, but the overall activation patterns were conserved across trials (Figure 2E, comparing middle and right). Consistent with several previous studies (King et al., 2013; Lee et al., 2018), we also noticed that the fraction of neurons activated by ultrasound varied between individual sessions and between animals. While majority of the sessions (65%, 15 of the 23 sessions) had less than 26% of neurons activated, 5 of the 23 sessions (22%) had over 50% neurons activated, and 3 had no activated neurons (Table 1). Since ultrasound stimulation was performed in awake animals with the transducer placed under the head, it is possible that slight difference in anatomical



| Table 1. Hippocampus response to ultrasound stimulation | | | | |
|---|-------------|----------------------------------|----------------------------|---------------------------------|
| Imaging session | Mouse ID | Number of total neurons recorded | Number of activated neuron | Percentage of activated neurons |
| 1 | 1 | 146 | 21 | 14.38 |
| 2 | 2 | 523 | 7 | 1.34 |
| 3 | 2 | 252 | 19 | 7.54 |
| 4 | 3 | 335 | 0 | 0 |
| 5 | 4 | 115 | 59 | 51.30 |
| 6 | 5 | 159 | 1 | 0.63 |
| 7 | 5 | 118 | 0 | 0 |
| 8 | 6 | 387 | 274 | 70.80 |
| 9 | 6 | 348 | 1 | 0.29 |
| 10 | 7 | 143 | 36 | 25.17 |
| 11 | 7 | 357 | 219 | 61.34 |
| 12 | 7 | 512 | 305 | 59.57 |
| 13 | 8 | 417 | 6 | 1.44 |
| 14 | 8 | 316 | 14 | 4.43 |
| 15 | 9 | 490 | 1 | 0.20 |
| 16 | 9 | 153 | 6 | 3.92 |
| 17 | 10 | 50 | 0 | 0 |
| 18 | 11 | 66 | 0 | 0 |
| 19 | 12 | 233 | 1 | 0.43 |
| 20 | 12 | 336 | 2 | 0.60 |
| 21 | 13 | 207 | 13 | 6.28 |
| 22 | 13 | 122 | 1 | 0.82 |
| 23 | 14 | 83 | 81 | 97.59 |

positions (jaw, chin, mouth, etc.) between individual animal could impact ultrasound transmission. It is also possible that the heterogeneity in CA1 neuron's biophysical properties and network states during awake conditions result in variable excitability of recorded neurons, which led to the variations in ultrasound evoked effects. Nonetheless, the existence of a large fraction of activated neurons in many recording sessions demonstrates that ultrasound stimulation when pulsed at the pattern described here can induce intracellular calcium increases within individual CA1 neurons.

To further confirm the effects of ultrasound stimulation, we performed sham stimulation on mice during GCaMP6 imaging without ultrasound gel, while maintaining all the other parameters the same as with the ultrasound stimulation group. The lack of ultrasound gel created an air gap between the transducer and the mouse head, and therefore, no ultrasound was transmitted into the brain. Upon sham stimulation, GCaMP6 intensity remained constant before and after stimulation across neurons (Figures 3A–3C, Table 2). Overall, the stimulation sessions exhibited higher percentages of activated neurons than the sham sessions (Wilcoxon rank-sum test, p = 0.0084). Only 6 out of 1545 neurons (0.4%, n = 1545 neurons recorded from 7 sessions in 3 mice, Table 2 and Figure 3D) were deemed activated using our statistical testing method (Wilcoxon rank-sum test, p < 0.05). This is in sharp contrast to the 18.2% activated neurons observed during ultrasound stimulation (Figure 2F and Table 1), and the fraction of activated neurons during sham stimulation was significantly lower than that during ultrasound stimulation (Fisher's Test, p < 0.001). Together, these results demonstrate that ultrasound stimulation activates a large fraction of individual neurons in the hippocampus.

Individual motor cortex neurons are activated by 100-ms-long pulsed ultrasound stimulation

To explore how different brain regions may be distinctly impacted by ultrasound, we imaged individual motor cortex neurons through surgically implanted imaging windows above the cortical surface, while





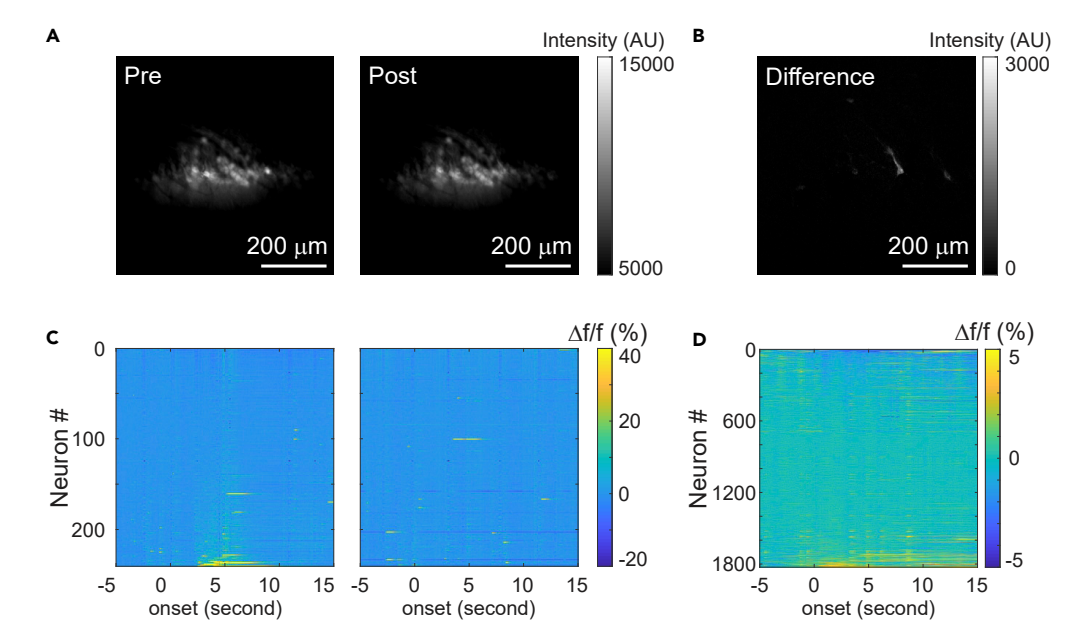


Figure 3. Individual hippocampal neuron responses upon sham ultrasound stimulation

- (A) Example intracellular GCaMP6 signal from hippocampal neurons before (left, max intensity projection of 5-s window) and immediately after (right, max intensity projection of 5-s window) sham stimulation. The images show 25% of total field of view.
- (B) The difference in intensity before and after sham stimulation.
- (C) GCaMP6 signals from the same field of view during two different trials, sorted in the same order.
- (D) Averaged response across 20 trials from all 1826 neurons, sorted from low to high by the averaged intensity during the 5-s window after sham stimulation. Each line represents an individual neuron.

performing ultrasound stimulation under the head, following the same protocol as described for the hippocampal experiments (Figures 1A and 1C). Similar to that observed in the hippocampus, many motor cortex neurons were activated by ultrasound, showing an increase in GCaMP6 fluorescence immediately after ultrasound onset, which peaked in a couple of seconds, and diminished \sim 5–10 s afterward (Figures 4A and 4B). Of the 651 neurons recorded, 279 (42.9%) were significantly activated by ultrasound (Figure 4F and Table 3, n = 651 neurons from 6 imaging sessions in 4 mice). In addition, we performed off-target stimulation by positioning the transducer underneath the abdomen instead of the head. We found that upon off-target simulation, only 4 of the total 1606 neurons (0.25%, n = 1606 neurons recorded from 5 sessions in 5 mice, Table 4) were activated, a significantly smaller fraction than that observed in the motor cortex when ultrasound was targeted to the head (Fisher's test, p < 0.001). This result further confirms that the ultrasound evoked responses in the motor cortex only occurred when the brain area was targeted by ultrasound stimulation directly.

Similar to that observed in the hippocampus, individual neurons in motor cortex also exhibited various responses to ultrasound stimulation across trials (Figures 4C and 4D). We further sorted simultaneously recorded neurons by ultrasound evoked responses across all 20 trials in one session (Figure 4E, left) and then plotted their corresponding GCaMP6 fluorescence during individual trials (Figure 4E, middle and right). Despite some variations in response at single trial level, the overall identify of the activated neurons is largely conserved across trials (Table 3).

Ultrasound stimulation evokes brain-region-specific responses

While individual neurons in both the hippocampus and the motor cortex were modulated by ultrasound stimulation, we noticed that ultrasound-induced responses observed in the motor cortex had higher amplitude and longer duration. To further compare the difference of ultrasound evoked responses between these two brain regions, we calculated the population response by averaging the GCaMP6 signals across all neurons. We found that ultrasound increases population GCaMP6 signals in both brain regions, whereas sham stimulation failed to alter population responses (Figure 5A). To estimate the latency of ultrasound



| Table 2. Hippocampus response to sham stimulation | | | | |
|---|-------------|----------------------------------|----------------------------|---------------------------------|
| Imaging session | Mouse ID | Number of total neurons recorded | Number of activated neuron | Percentage of activated neurons |
| 1 | 15 | 218 | 1 | 0.46 |
| 2 | 15 | 240 | 0 | 0 |
| 3 | 15 | 126 | 0 | 0 |
| 4 | 15 | 142 | 0 | 0 |
| 5 | 16 | 105 | 0 | 0 |
| 6 | 3 | 439 | 5 | 1.14 |
| 7 | 3 | 275 | 0 | 0 |

evoked responses, we calculated the averaged GCaMP6 responses across only the activated neuron populations in the hippocampus and the motor cortex and identified the latency as the time point when the averaged population responses exceeded two standard deviations above the baseline (Figure 5B). We found that ultrasound activated hippocampus CA1 within 50 ms after ultrasound onset, leading to significantly increased fluorescence in the very first image frame after ultrasound onset. The estimation of activation latency is limited by the 20 Hz, 50 ms per frame image acquisition rate (Figure 5B, blue). In the motor cortex, however, we noted a transient ultrasound-induced tissue displacement, which reduced GCaMP6 signals when fluorescently labeled neurons moved out of the imaging focal plane during the 100-mslong ultrasound stimulation, resulting in a latency estimation of 350 ms (Figure 5B, red). This ultrasound-induced tissue displacement was only observed in the motor cortex but not in the hippocampus, likely due to the surgical preparation of the motor cortex imaging chamber on top of the brain surface that is less stable than the hippocampal imaging chamber deeply embedded within the brain tissue.

To further characterize the difference in evoked calcium responses across individual neurons in the two brain regions, we calculated the peak of trial averaged GCaMP6 fluorescence within the response period (peak amplitude), the time when the evoked GCaMP6 fluorescence reached the peak amplitude (peak timing), and the duration when evoked GCaMP6 fluorescence remained above 50% of the peak amplitude (activation duration). We then compared these properties between the 1065 activated hippocampal neurons and the 279 activated motor cortex neurons. We found that ultrasound evoked calcium events in the hippocampal neurons had a peak timing of 2.81 \pm 0.90 s (mean \pm standard deviation) after ultrasound onset (Figure 5C), an activation duration of 4.97 ± 4.08 s (mean \pm standard deviation, Figure 5D) and a peak amplitude of 2.17 \pm 1.82% (mean \pm standard deviation, Figure 5E). In contrast, ultrasound-induced calcium events in motor cortex neurons had a peak timing of 3.26 \pm 0.79 s (mean \pm standard deviation, Figure 5F), 0.45 s later than that detected in the hippocampus. Additionally, motor cortex evoked events had a much longer activation duration of 7.39 \pm 2.12 s (mean \pm standard deviation, Figure 5G), 2.42 s longer than the hippocampus. Finally, motor cortex evoked events reached a much larger peak amplitude of 5.73 \pm 1.84% (mean \pm standard deviation, Figure 5H), 264% of that detected in the hippocampus. Overall, the activation profiles from motor cortex are slower, wider, and larger than those from the hippocampus, indicating a region-specific effect when ultrasound neuromodulation was delivered as described here (two-sample Kolmogorov-Smirnov test; peak timing p = 3.0993×10^{-44} ; activation duration p = 1.7300×10^{-44} 10^{-60} ; peak amplitude p = 9.0568 × 10^{-117}).

Our computational simulation results indicated that the instantaneous pressure in the motor cortex was 8.2% more than that in the hippocampus (Figures 1B and 1C), which may lead to some variation in evoked response amplitude between the two areas, but this small ultrasound pressure difference is unlikely to account for the observed 264% higher amplitude observed in the motor cortex than the hippocampus. In addition, variation in acoustic pressure during the brief 100-ms-long ultrasound stimulation period cannot account for the large temporal difference of seconds as observed between the two brain regions. Together, these results provide direct evidence that ultrasound stimulation evokes distinct neural activation profiles between the two brain regions examined.

DISCUSSION

In recent years, ultrasound neuromodulation has been increasingly explored as a promising noninvasive brain stimulation technique. While many studies have characterized the neuromodulation effects of



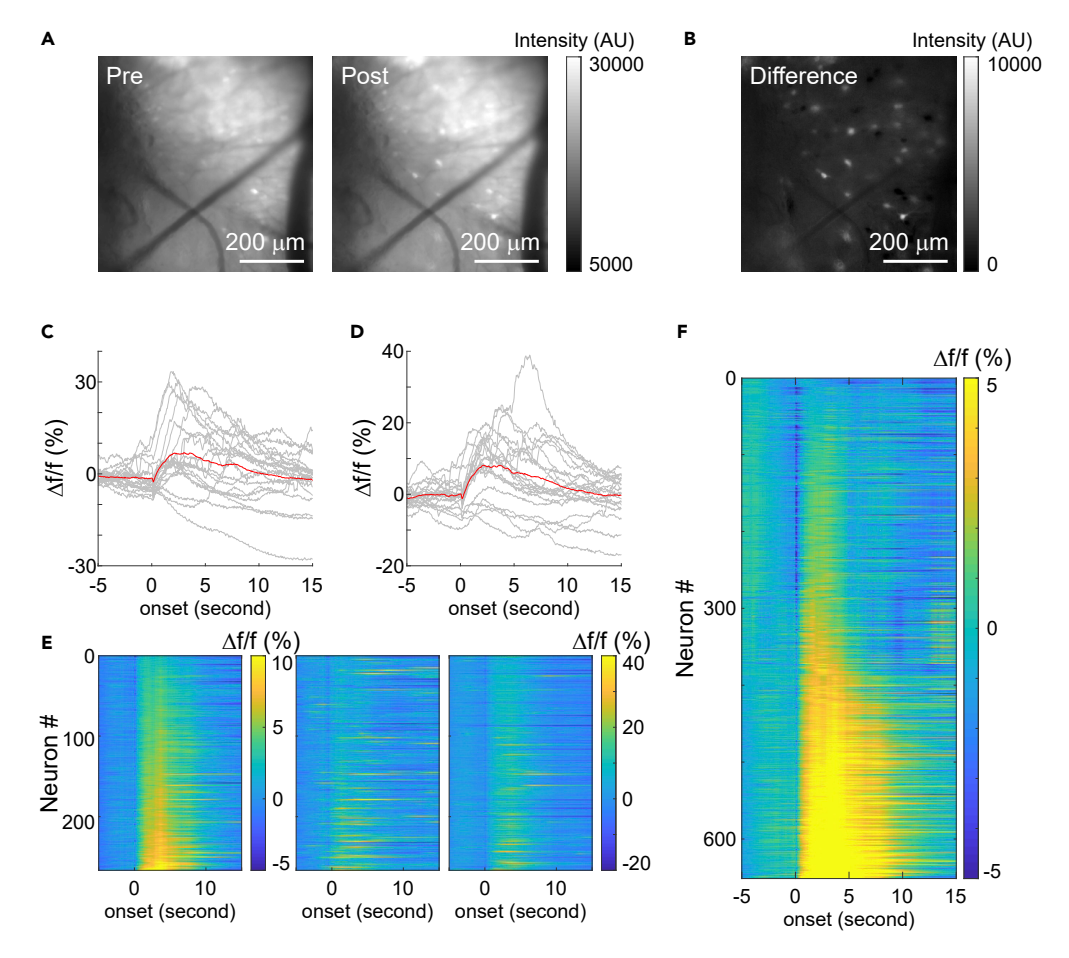


Figure 4. Individual motor cortex neurons are activated by pulsed ultrasound stimulation

(A) Example intracellular GCaMP6 signals from neurons in motor cortex before (left, max intensity projection of 5-s window) and immediately after (right, max intensity projection of 5-s window) ultrasound stimulation. The images show 25% of total field of view.

(B) The difference in GCaMP6 intensity before and after stimulation. The bright neurons indicated the increase in intracellular calcium concentration in respond to ultrasound stimulation.

(C and D) GCaMP6 signals from two example neurons during ultrasound stimulation, aligned to the stimulation onset. Each gray line represents a single trial, and the red line represents the average response across all 20 trials.

(E) Averaged GCaMP6 signals from neurons in the same field of view over 20 trials (left), and during two example trials (middle and right) in the same imaging session. Neurons were sorted based the fluorescence intensity of the averaged signals during the 5-s window after ultrasound.

(F) Averaged responses across 20 trials from 651 neurons in the motor cortex, sorted from low to high by the averaged intensity during the 5-s window after ultrasound stimulation. Each line represents an individual neuron.

ultrasound on neural activities using indirect methods by measuring muscle EMG, BOLD signals with fMRI or fNIR, or bulk electrophysiological measures of LFPs or EEGs (Legon et al., 2012; Kim et al., 2017; Yuan et al., 2020), few studies have examined the effect of ultrasound on individual neurons in intact brain environment. Here, we investigated the effect of ultrasound on modulating intracellular calcium concentration of individual neurons in awake mice, free of anesthesia effect, using a large-scale single-neuron calcium imaging technique. We quantified ultrasound-evoked responses across multiple stimulation trials, and experimental sessions in two brain regions, the hippocampus and the motor cortex. Our results demonstrate that ultrasound evokes transient and immediate increases in intracellular calcium in a large fraction of individual neurons in both brain regions, with an onset latency of less than 50 ms in the hippocampus. Ultrasound-evoked hippocampus responses were significantly shorter in duration and smaller in magnitude than those observed in the motor cortex, demonstrating that ultrasound evokes distinct neural activation profiles in the two brain regions when delivered non-invasively as described here.





| Table 3. Motor cortex response to ultrasound stimulation | | | | |
|--|-------------|----------------------------------|----------------------------|---------------------------------|
| Imaging session | Mouse ID | Number of total neurons recorded | Number of activated neuron | Percentage of activated neurons |
| 1 | 22 | 266 | 240 | 90.23 |
| 2 | 22 | 167 | 13 | 7.78 |
| 3 | 23 | 38 | 0 | 0 |
| 4 | 23 | 87 | 11 | 12.64 |
| 5 | 24 | 65 | 0 | 0 |
| 6 | 25 | 28 | 15 | 53.57 |

Given that our study was performed in the brain of awake animals, where the excitability of individual neurons is influenced by both local environment and synaptic inputs from the connected brain areas, it is not surprising that ultrasound-evoked responses exhibit some levels of trial-by-trial variations and session-by-session variations. It is known that individual ion channel activation follows probability distributions, and the membrane potentials of individual neurons are intrinsically noisy. On many occasions, the noisy nature of membrane potential plays a crucial role in generating action potentials. Since one possible mechanism for ultrasound stimulation is via mechanosensitive ion channels, ultrasound could increase the probability of channel opening, instead of simply activating the channel in an all-or-none manner, resulting in a non-deterministic GCaMP6 response at the individual trial level. Such variation in single neuron biophysics, coupled with variation in connectivity strength between neurons within a network would create additional heterogeneity in excitability. As consistently observed in most systems neuroscience studies, a specific behavior paradigm recruits different subsets of neurons in the same brain region to generate the same behavioral outcome. It is therefore plausible that even though ultrasound stimulation activates slightly different subsets of neurons in different trials, it could still produce similar downstream effects, such as inducing motor activities, as observed in previous studies.

Two recent studies demonstrated that ultrasound stimulation can vibrate cochlear fluid in anesthetized animals leading to changes in downstream cortical regions several hundred ms after ultrasound onset (Sato et al., 2018; Guo et al., 2018). However, conflicting results were also reported where the effects of ultrasound stimulation were detected in transgenetically deaf mice, supporting direct ultrasound modulation of neurons in the mouse brain (Mohammadjavadi et al., 2019). In our study, we detected that ultrasound activates hippocampal CA1 neurons with a much shorter latency of under 50 ms, and our latency estimation is limited by the 20 Hz, 50 ms per frame image acquisition rate. Hippocampus is classically considered the learning and memory center of the brain and is not known to have robust auditory or visual evoked responses. Furthermore, the hippocampus, being a highly cognitive area of the brain, exhibits sparse responses even in learning and memory studies designed to evoke hippocampal responses. For example, in our recent calcium imaging studies, we found that less than 15% of CA1 neurons were activated in mice that have acquired an auditory dependent trace conditioning learning task, and very few CA1 neurons responded to auditory stimulation in the absence of learning (Mount et al., 2021). In contrast, we here detected 18% of CA1 neurons being activated by ultrasound stimulation, while mice were awake and head-fixed without being engaged in any behavioral task. While it is unclear whether the evoked intracellular calcium increase in individual CA1 neurons is related to action potentials, the fact that ultrasound can modulate CA1 neurons' intracellular calcium provides a unique aspect of ultrasound modulation effects via intracellular signaling pathways. Together, the short latency of ultrasound-evoked CA1 responses and the large fraction of activated CA1 neurons demonstrate that ultrasound can produce direct effect on individual neurons in the intact brain.

We detected an increase in intracellular calcium concentration in individual motor cortex neurons 350 ms after ultrasound onset. This latency estimation in the motor cortex was impacted by ultrasound-induced tissue displacement, likely due to the stability of the surgically implanted imaging chamber, resulting in transient reduction of GCaMP6 fluorescence at ultrasound onset. Nonetheless, the short latency response observed in the motor cortex is unlikely explained by indirect auditory pathway activation that resulted in visual cortex activation several hundred ms after ultrasound onset as reported in Sato et al. (Sato et al., 2018). The differences between the response profile evoked by ultrasound stimulation in the two brain regions also indicate that the observed responses were not merely motion artifacts caused by animal locomotion, which would result in a similar pattern of intensity reduction across all brain regions. The latency of





| Table 4. Motor cortex response to off-target ultrasound stimulation to the abdomen | | | | |
|--|-------------|----------------------------------|----------------------------|---------------------------------|
| Imaging session | Mouse ID | Number of total neurons recorded | Number of activated neuron | Percentage of activated neurons |
| 1 | 17 | 130 | 0 | 0 |
| 2 | 18 | 330 | 0 | 0 |
| 3 | 19 | 269 | 2 | 0.74 |
| 4 | 20 | 437 | 2 | 0.46 |
| 5 | 21 | 440 | 0 | 0 |

the evoked calcium response observed here in individual neurons in the awake brain is interestingly consistent with that observed in a recent *in vitro* calcium imaging study, where ultrasound-evoked calcium increase in cultured neurons had a delay of about 200 ms (Yoo et al., 2020), further highlighting that ultrasound effects observed here are through direct modulation of neurons.

We observed that the ultrasound evoked hippocampal responses are shorter in duration and smaller in amplitude than that seen in the motor cortex. Ultrasound stimulation, when delivered noninvasively, is subject to modulation by brain structures with different acoustic properties, such as cranial bones, blood vessels, membranes, and cerebrospinal fluid content, which results in heterogeneity in intensity distribution in the brain. Our computational simulation results indicated that motor cortex received 8.2% more ultrasound power than the hippocampus during the brief 100-ms period when ultrasound was delivered. This small variation in ultrasound intensity between the two brain areas is unlikely to account for the 264% difference in response amplitude, and the several-second-long variations in response duration detected in the two brain regions. While our computational simulation cannot capture detailed brain structural variations and thus may underestimate the intensity difference between the two regions studied, it is unlikely that such underestimation would be large enough to account for the 264% difference in the evoked response amplitude detected between the two brain regions. Finally, even if the intensity differences could contribute to some of the amplitude variations observed between the two brain regions, such intensity difference during the brief 100-ms-long ultrasound stimulation period cannot explain the 2.42-s-long difference in activation duration detected in the two brain regions. Thus, the difference in ultrasoundevoked responses detected in the hippocampus and the motor cortex is due to brain-region-specific tissue properties. Recently fMRI studies in nonhuman primates showed that focused ultrasound stimulation of somatosensory cortex produces either excitatory or inhibitory effects in the brain depending on the activity states of the somatosensory pathway (Yang et al., 2021). Our observation of brain-region-specific ultrasound neuromodulation effect further highlights that neural circuit properties are critical consideration in ultrasound neuromodulation. Thus, the effect of ultrasound neuromodulation in intact brain not only depends on the acoustic profiles of ultrasound waveforms but also the specific tissue structure of the local environment including neural tissue architecture, vasculature and cranial bone structure, and the functional connectivity patterns and activation states of neural circuits. As ultrasound is increasingly considered a potential therapeutic technique for noninvasive neural stimulation, these results highlight the need of further investigation of the relationship between ultrasound propagation in the intact brain and the region-specific and state-dependent neuromodulation effect.

It is also important to understand the cellular mechanisms of ultrasound neuromodulation in the brain, especially given the promising translational potentials of ultrasound neuromodulation. Many *in vitro* studies have suggested that mechanosensitive channels can mediate ultrasound-evoked neuron responses, and *in vivo* studies demonstrated that neurons in intact neural circuits and fluidic tissue structures are sensitive to the mechanical pressure generated by ultrasound stimulation (Li et al., 2016; Kubanek et al., 2016, 2018). It is highly plausible that different neural circuits can be activated by ultrasound with varying thresholds. Further studies using single-cell measurement techniques as demonstrated here could help provide mechanistic insights on how individual neurons are sensitized by ultrasound in the intact brain and whether different neuron types in different brain regions may be selectively recruited by specific ultrasound stimulation parameters.

Limitations of the study

The utilization of high-performance calcium sensors and large-area widefield microscopy allowed us to characterize ultrasound evoked responses from a large number of neurons in different brain regions in awake mice, at single-neuron level and with a temporal precision of 50 ms. Intracellular calcium plays key roles in regulating signaling pathways in neurons, and somatic calcium concentration is modulated



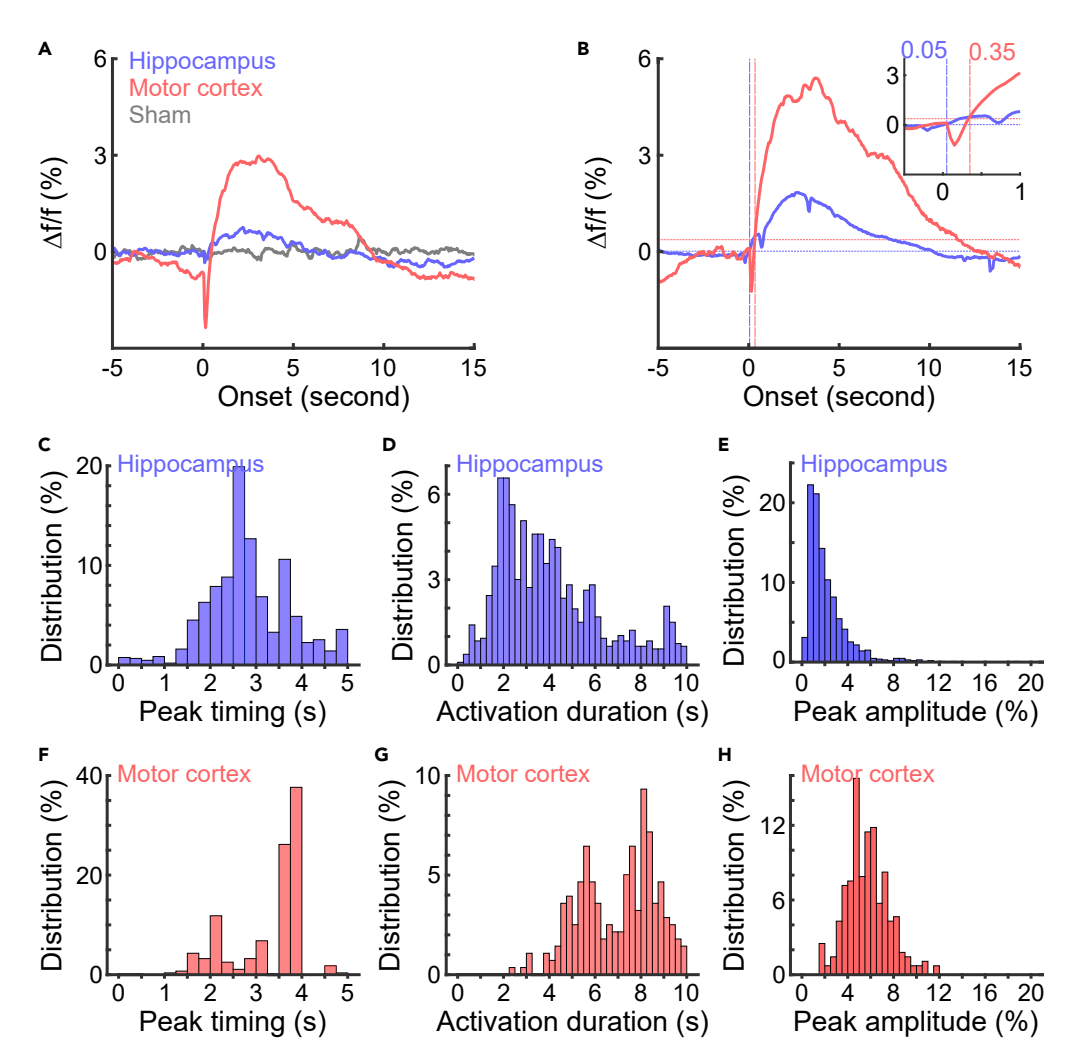


Figure 5. Brain region specific activation by ultrasound stimulation

(A) The population response of all hippocampal neurons and all motor cortex neurons during ultrasound stimulation (blue and red, respectively) and during sham stimulation (gray).

(B) Ultrasound evoked responses, calculated as the average responses from positively modulated neurons in the hippocampus (blue) and in the motor cortex (red). The horizonal lines indicate the activation threshold to determine onset latency. The vertical lines indicate the response latency (blue: hippocampus, red: motor cortex).

- (C) The distribution of the peak timing of ultrasound evoked responses in hippocampal neurons.
- (D) The distribution of the activation duration of ultrasound evoked responses in hippocampal neurons.
- (E) The distribution of the peak amplitude of ultrasound evoked responses in hippocampal neurons.
- (F) The distribution of the peak timing of ultrasound evoked responses in motor cortex neurons.
- (G) The distribution of the activation duration of ultrasound evoked responses in motor cortex neurons.
- (H) The distribution of the peak amplitude of ultrasound evoked responses in motor cortex neurons.

by action potentials. However, the relationship between action potentials and intracellular somatic calcium is complex and nonlinear (Huang et al., 2021). It is thus unclear to what degree the ultrasound evoked increases in intracellular calcium observed here are related to action potentials. Previous *in vitro* studies demonstrated that blocking action potential generation in neurons attenuated, but did not eliminate, ultrasound evoked intracellular calcium increases in brain slices (Tyler et al., 2008) and in cultured neurons (Yoo et al., 2020). Additionally, ultrasound stimulation was shown to increase intracellular calcium concentration in astrocytes, a cell type that does not generate action potentials (Oh et al., 2020). Our observation that ultrasound stimulation increases intracellular calcium concentration in individual neurons in awake mice highlights that ultrasound neuromodulation can alter neural circuit function through intracellular calcium, regardless of its effect on membrane voltage. Future studies combining single-cell voltage





measurement (Piatkevich et al., 2019) and calcium measurement will help dissociate ultrasound effects on membrane voltage versus intracellular calcium.

STAR*METHODS

Detailed methods are provided in the online version of this paper and include the following:

- KEY RESOURCES TABLE
- RESOURCE AVAILABILITY
 - Lead contact
 - Materials availability
 - O Data and code availability
- EXPERIMENTAL MODEL AND SUBJECT DETAILS
- METHOD DETAILS
 - Animal preparation
 - O Wide-field calcium imaging and ultrasound stimulation
 - O Calcium imaging data analysis: motion correction
 - Calcium imaging data analysis: regions of interest (ROI) segmentation, and fluorescence trace extraction
 - O Calcium imaging data analysis: identification of activated individual neurons
 - Calcium imaging data analysis: characterization of activation profiles in the hippocampus and the motor cortex
 - O Simulation of ultrasound intensity distribution in the brain

ACKNOWLEDGMENTS

We thank members of Han lab for technical support throughout the project and for providing comments to the manuscript.

X.H. acknowledges funding from DARPA Young Faculty Award, NIH (1R01NS109794 and 1R01NS115797), and NSF 1848029. J.S. acknowledges funding from 5T32GM008541-23, and E.B. acknowledges NSF grant # DGE-1840990.

AUTHOR CONTRIBUTIONS

H.T. and X.H. designed all the experiments. H.T., J.S. and A.M. collected animal data. J.S., A.M., H.J.G. and S.B. performed animal preparations. E.B., R.T, and T. S performed computational simulation, H.T. and D.Z. curated the training data for deep learning network. H.T. performed all the analysis. X.H. supervised the study. H.T. and X.H. wrote the manuscript, and all authors edited the manuscript.

DECLARATION OF INTERESTS

The authors declare no competing interests.

Received: October 16, 2020 Revised: March 31, 2021 Accepted: August 3, 2021 Published: September 24, 2021

REFERENCES

Chan, E., Kovacevic, N., Ho, S.K., Henkelman, R.M., and Henderson, J.T. (2007). Development of a high resolution three-dimensional surgical atlas of the murine head for strains 129S1/SvImJ and C57BI/6J using magnetic resonance imaging and micro-computed tomography. Neuroscience 144, 604–615.

Dinno, M.A., Dyson, M., Young, S.R., Mortimer, A.J., Hart, J., and Crum, L.A. (1989). The significance of membrane changes in the safe and effective use of therapeutic and diagnostic ultrasound. Phys. Med. Biol. *34*, 1543–1552.

Fini, M., and Tyler, W.J. (2017). Transcranial focused ultrasound: a new tool for non-invasive neuromodulation. Int. Rev. Psychiatry *29*, 168–177.

Fry, F.J., Ades, H.W., and Fry, W.J. (1958). Production of reversible changes in the central nervous system by ultrasound. Science 127, 83–84

Gavrilov, L.R., Gersuni, G.V., Ilyinsky, O.B., Sirotyuk, M.G., Tsirulnikov, E.M., and Shchekanov, E.E. (1976). The effect of focused ultrasound on the skin and deep nerve structures of man and animal. Prog. Brain Res. 43, 279–292.

Guo, H., Hamilton, M., 2nd, Offutt, S.J., Gloeckner, C.D., Li, T., Kim, Y., Legon, W., Alford, J.K., and Lim, H.H. (2018). Ultrasound produces extensive brain activation via a cochlear pathway. Neuron *98*, 1020–1030 e4.

Harvey, E.N. (1929). The effect of high frequency sound waves on heart muscle and other irritable tissues. Am. J. Physiol. *91*, 284–290.

iScience

Article



Huang, L., Ledochowitsch, P., Knoblich, U., Lecoq, J., Murphy, G.J., Reid, C., De Vries, S.E.J., Koch, C., Zeng, H., Buice, M.A., et al. (2021). Relationship between simultaneously recorded spiking activity and fluorescence signal in GCaMP6 transgenic mice. Elife 10, e51675.

Kaye, G.W.C., and Laby, T.H. (1995). Tables of physical and chemical constants (Longman Sc & Tech).

Kim, E., Anguluan, E., and Kim, J.G. (2017). Monitoring cerebral hemodynamic change during transcranial ultrasound stimulation using optical intrinsic signal imaging. Sci. Rep. 7, 13148.

King, R.L., Brown, J.R., Newsome, W.T., and Pauly, K.B. (2013). Effective parameters for ultrasound-induced in vivo neurostimulation. Ultrasound Med. Biol. *39*, 312–331.

Krasovitski, B., Frenkel, V., Shoham, S., and Kimmel, E. (2011). Intramembrane cavitation as a unifying mechanism for ultrasound-induced bioeffects. Proc. Natl. Acad. Sci. US A 108, 3258–3263.

Kubanek, J., Shi, J., Marsh, J., Chen, D., Deng, C., and Cui, J. (2016). Ultrasound modulates ion channel currents. Sci. Rep. 6, srep24170.

Kubanek, J., Shukla, P., Das, A., Baccus, S.A., and Goodman, M.B. (2018). Ultrasound elicits behavioral responses through mechanical effects on neurons and ion channels in a simple nervous system. J. Neurosci. *38*, 3081–3091.

Lee, W., Croce, P., Margolin, R.W., Cammalleri, A., Yoon, K., and Yoo, S.S. (2018). Transcranial focused ultrasound stimulation of motor cortical areas in freely-moving awake rats. BMC Neurosci. 19. 57.

Lee, W., Kim, H., Jung, Y., Song, I.U., Chung, Y.A., and Yoo, S.S. (2015). Image-guided transcranial focused ultrasound stimulates human primary somatosensory cortex. Sci. Rep. 5, 8743.

Lee, W., Kim, H.C., Jung, Y., Chung, Y.A., Song, I.U., Lee, J.H., and Yoo, S.S. (2016). Transcranial focused ultrasound stimulation of human primary visual cortex. Sci. Rep. 6, 34026.

Legon, W., Rowlands, A., Opitz, A., Sato, T.F., and Tyler, W.J. (2012). Pulsed ultrasound differentially stimulates somatosensory circuits in humans as indicated by EEG and FMRI. PLoS One 7, e51177.

Legon, W., Sato, T.F., Opitz, A., Mueller, J., Barbour, A., Williams, A., and Tyler, W.J. (2014). Transcranial focused ultrasound modulates the activity of primary somatosensory cortex in humans. Nat. Neurosci. 17, 322–329.

Li, G.F., Zhao, H.X., Zhou, H., Yan, F., Wang, J.Y., Xu, C.X., Wang, C.Z., Niu, L.L., Meng, L., Wu, S., et al. (2016). Improved anatomical specificity of non-invasive neuro-stimulation by high frequency (5 MHz) ultrasound. Sci. Rep. 6, 24738.

Lin, J.W., Yu, F., Muller, W.S., Ehnholm, G., and Okada, Y. (2019). Focused ultrasound transiently

increases membrane conductance in isolated crayfish axon. J. Neurophysiol. 121, 480–489.

Menz, M.D., Oralkan, O., Khuri-Yakub, P.T., and Baccus, S.A. (2013). Precise neural stimulation in the retina using focused ultrasound. J. Neurosci. 33, 4550–4560.

Mohammadjavadi, M., Ye, P.P., Xia, A., Brown, J., Popelka, G., and Pauly, K.B. (2019). Elimination of peripheral auditory pathway activation does not affect motor responses from ultrasound neuromodulation. Brain Stimul. 12, 901–910.

Mohammed, A.I., Gritton, H.J., Tseng, H.A., Bucklin, M.E., Yao, Z., and Han, X. (2016). An integrative approach for analyzing hundreds of neurons in task performing mice using wide-field calcium imaging. Sci. Rep. 6, 20986.

Mount, R.A., Sridhar, S., Hansen, K.R., Mohammed, A.I., Abdulkerim, M., Kessel, R., Nazer, B., Gritton, H.J., and Han, X. (2021). Distinct neuronal populations contribute to trace conditioning and extinction learning in the hippocampal CA1. Elife 10, e56491.

Mueller, J.K., Ai, L., Bansal, P., and Legon, W. (2017). Numerical evaluation of the skull for human neuromodulation with transcranial focused ultrasound. J. Neural Eng. 14, 066012.

Oh, S.J., Lee, J.M., Kim, H.B., Lee, J., Han, S., Bae, J.Y., Hong, G.S., Koh, W., Kwon, J., Hwang, E.S., et al. (2020). Ultrasonic neuromodulation via astrocytic TRPA1. Curr. Biol. *30*, 948.

Piatkevich, K.D., Bensussen, S., Tseng, H.A., Shroff, S.N., Lopez-Huerta, V.G., Park, D., Jung, E.E., Shemesh, O.A., Straub, C., Gritton, H.J., et al. (2019). Population imaging of neural activity in awake behaving mice. Nature 574, 413–417.

Plaksin, M., Kimmel, E., and Shoham, S. (2016). Cell-type-selective effects of intramembrane cavitation as a unifying theoretical framework for ultrasonic neuromodulation. eNeuro 3. https://doi.org/10.1523/ENEURO.0136-15.2016.

Ronneberger, O., Fischer, P., and Brox, T. (2015). U-net: convolutional networks for biomedical image segmentation. https://ui.adsabs.harvard.edu/abs/2015arXiv150504597R.

Sato, T., Shapiro, M.G., and Tsao, D.Y. (2018). Ultrasonic neuromodulation causes widespread cortical activation via an indirect auditory mechanism. Neuron *98*, 1031–1041.e5.

Shen, S.P., Tseng, H.A., Hansen, K.R., Wu, R., Gritton, H.J., Si, J., and Han, X. (2018). Automatic cell segmentation by adaptive thresholding (ACSAT) for large-scale calcium imaging datasets. eNeuro 5. https://doi.org/10.1523/ENEURO.0056-18.2018.

Szabo, T.L. (1995). Causal theories and data for acoustic attenuation obeying a frequency power law. J. Acoust. Soc. America 97, 14–24.

Szabo, T.L. (2014). DIAGNOSTIC ULTRASOUND IMAGING: Inside Out, Second edition (Elsevier).

Ter Haar, G. (2007). Therapeutic applications of ultrasound. Prog. Biophys. Mol. Biol. 93, 111–129.

Treeby, B.E., and Cox, B.T. (2010). k-Wave: MATLAB toolbox for the simulation and reconstruction of photoacoustic wave fields. J. Biomed. Opt. 15, 021314.

Tufail, Y., Matyushov, A., Baldwin, N., Tauchmann, M.L., Georges, J., Yoshihiro, A., Tillery, S.I., and Tyler, W.J. (2010). Transcranial pulsed ultrasound stimulates intact brain circuits. Neuron *66*, 681–694.

Tufail, Y., Yoshihiro, A., Pati, S., Li, M.M., and Tyler, W.J. (2011). Ultrasonic neuromodulation by brain stimulation with transcranial ultrasound. Nat. Protoc. *6*, 1453–1470.

Tyler, W.J. (2012). The mechanobiology of brain function. Nat. Rev. Neurosci. 13, 867–878.

Tyler, W.J., Tufail, Y., Finsterwald, M., Tauchmann, M.L., Olson, E.J., and Majestic, C. (2008). Remote excitation of neuronal circuits using low-intensity, low-frequency ultrasound. PLoS One 3, e3511.

Velling, V.A., and Shklyaruk, S.P. (1988). Modulation of the functional state of the brain with the aid of focused ultrasonic action. Neurosci. Behav. Physiol. 18, 369–375.

White, P.J., Clement, G.T., and Hynynen, K. (2006). Longitudinal and shear mode ultrasound propagation in human skull bone. Ultrasound Med. Biol. *32*, 1085–1096.

Yang, F.Y., Lu, W.W., Lin, W.T., Chang, C.W., and Huang, S.L. (2015). Enhancement of neurotrophic factors in astrocyte for neuroprotective effects in brain disorders using low-intensity pulsed ultrasound stimulation. Brain Stimul. 8, 465–473.

Yang, P.F., Phipps, M.A., Jonathan, S., Newton, A.T., Byun, N., Gore, J.C., Grissom, W.A., Caskey, C.F., and Chen, L.M. (2021). Bidirectional and state-dependent modulation of brain activity by transcranial focused ultrasound in non-human primates. Brain Stimul. 14, 261–272.

Yang, P.F., Phipps, M.A., Newton, A.T., Chaplin, V., Gore, J.C., Caskey, C.F., and Chen, L.M. (2018). Neuromodulation of sensory networks in monkey brain by focused ultrasound with MRI guidance and detection. Sci. Rep. 8, 7993.

Ye, P.P., Brown, J.R., and Pauly, K.B. (2016). Frequency dependence of ultrasound neurostimulation in the mouse brain. Ultrasound Med. Biol. 42, 1512–1530.

Yoo, S., Mittelstein, D.R., Hurt, R., Lacroix, J., and Shapiro, M.G. (2020). Focused ultrasound excites neurons via mechanosensitive calcium accumulation and ion channel amplification.

Yuan, Y., Wang, Z., Liu, M., and Shoham, S. (2020). Cortical hemodynamic responses induced by low-intensity transcranial ultrasound stimulation of mouse cortex. Neuroimage *211*, 116597.





STAR*METHODS

KEY RESOURCES TABLE

| REAGENT or RESOURCE | SOURCE | IDENTIFIER |
|-----------------------------|--|------------|
| Bacterial and virus strains | | |
| AAV9-syn-GCaMP6f | University of Pennsylvania Vector Core | N/A |
| AAV9-syn-jGCaMP7f | Addgene.org | N/A |
| Software and algorithms | | |
| Matlab 2018b | MathWork | SCR001622 |
| Python | Python.org | SCR008394 |
| Tensorflow | Google | N/A |
| Keras | keras.io | N/A |
| SciPy | scipy.org | N/A |
| NumPy | numpy.org | N/A |
| Imgaug | https://github.com/aleju/imgaug | N/A |
| h5py | h5py.org | N/A |
| Matplotlib | matplotlib.org | N/A |
| PIL | https://python-pillow.org/ | N/A |
| Skimage | scikit-image.org | N/A |
| Tifffile | https://pypi.org/project/tifffile/ | N/A |
| Tqdm | https://github.com/tqdm/tqdm | N/A |
| HCImage Live | Hamamatsu | N/A |
| k-Wave acoustic toolbox | http://www.k-wave.org/ | N/A |

RESOURCE AVAILABILITY

Lead contact

Resources related to this study are available upon reasonable request from the Lead Contact (Xue Han, xuehan@bu.edu).

Materials availability

AAV viral vectors used in this study are available at Addgene.org and University of Pennsylvania Vector Core.

Data and code availability

The data and the code used in this study are available upon reasonable request from the Lead Contact (Xue Han, xuehan@bu.edu).

EXPERIMENTAL MODEL AND SUBJECT DETAILS

All procedures were performed in accordance with the National Institutes of Health Guide for Laboratory Animals and were approved by Boston University Institutional Animal Care and Use Committee. Adult female C57BL/6 mice (Charles River Laboratories) were used for the study.

METHOD DETAILS

Animal preparation

All procedures were performed in accordance with the National Institutes of Health Guide for Laboratory Animals and were approved by Boston University Institutional Animal Care and Use Committee and Biosafety Committee. Window implantation surgeries were performed on adult female C57BL/6 mice (Charles River Laboratories) aged 8-12 weeks, following standard aseptic surgery and postoperative care procedures. Imaging windows were constructed by fixing a glass coverslip (no. 0, OD: 3mm, Deckgläser



Cover Glasses, Warner Instruments, 64-0726 (CS-3R-0)) to the bottom of a metal cannula (OD: 3.17mm, ID: 2.36mm, height 1mm or 2mm AmazonSupply, B004TUE45E) with an ultraviolet curable optical adhesive (Norland Products). A virus infusion cannula (26G, PlasticsOne, C135GS-4/SPC) was attached to the side of the imaging window at a 45 angle. Hippocampal imaging windows, cover glasses affixed to the 2mm long metal cannula, were positioned over the hippocampus (AP: -2.0 mm, ML: +2.0 mm), with the overlaying cortical tissue aspirated. Motor cortex imaging windows, cover glass with or without 1mm long metal cannula, were positioned over the motor cortex surface (AP: +1.5 mm, ML: ± 1.75 mm), laying above dura. Imaging windows were affixed to the skull with C&B metabond (S380, Patterson Dental, Saint Paul, MN), along with a custom aluminum head fixation bar. One week following window implantation, 750nL of AAV9-syn-GCaMP6f (University of Pennsylvania Vector Core, titer \sim 6e12vg/mL) was administered through the infusion cannulas at a flow rate of 100nl/min in both the hippocampus and the motor cortex. For the off-target ultrasound stimulation experiment, AAV9-syn-jGCaMP7f (Addgene, titer \sim 1e13vg/mL) was infused into the motor cortex before implanting imaging window. Fluorescence calcium imaging sessions were performed at least 7 days after viral infusion to allow for adequate GCaMP expression.

Wide-field calcium imaging and ultrasound stimulation

Calcium imaging was acquired with a custom wide-field microscope as described in our previous study (Mohammed et al., 2016). Briefly, the microscope includes a scientific CMOS camera (ORCA-Flash4.0 LT Digital CMOS camera C11440-42U; Hamamatsu, Boston, MA), a Leica N Plan 10x0.25 PH1 or a Mitutoyo 10x M Plan APO objective lens, a 460 nm LED (LZ1-00B200; LedEngin, San Jose CA), an excitation filter (FF01-468/553-25; Semrock, Rochester, NY), a dichronic (FF493/574-Di01-25x36; Semrock, Rochester, NY), an emission filter (FF01-512/630-25; Semrock, Rochester, NY), and a tube lens (Nikon Zoom-NIKKOR 80-200mm f/4 Al-s). The objective lens used here are air coupled. Fluorescence images were acquired at 20 Hz with HCImage live (Hamamatsu; Boston, MA), with the sCMOS cameras binned to 1024x1024 pixels, corresponding to $1.312x1.312 \,\mu\text{m}^2/\text{pixel}$, and a total field of view size of $1.343x1.343 \,\text{mm}^2$

During each imaging session, mice were awake, head-fixed using surgically implanted head fixation bars (Figure 1). A commercial ultrasound transducer (GS350-D13, The Ultra Group Inc, PA) was placed under the head via a custom 3D printed holder that allowed for complete filling of ultrasound gel between the ultrasound transducer and the animal to ensure proper transfer of ultrasound to the head or the abdomen. Each imaging session consisted of 20 ultrasound stimulation trials, and each trial lasted for 30 or 60 seconds long. Ultrasound was triggered by the sCOMS camera 10 second after trial started, and ultrasound waveforms were generated by two function generators (33220A Agilent CA). The first function generator received the trigger signal from the camera, and then sent out 200 cycles of pulses at 2 kHz to the second function generator, which subsequently outputted 75 cycles of sine waves at 350 kHz to an amplifier (AG1006 T&C Power, NY) connected to the transducer. The stimulation protocol was based on Tufail et al. (Tufail et al., 2011). Ultrasound power was verified with a needle hydrophone (NH2000 Precision Acoustics Ltd, UK). During experiments, the ultrasound amplifier was set at 70% of its maximum power, resulting a transducer output at ~0.44 MPa at the end of the near field.

Calcium imaging data analysis: motion correction

Calcium imaging data analysis was performed offline. Calcium imaging video of each recording session, including multiple trials, was first motion corrected using a custom Python script. We first generated a reference image by averaging pixel intensities across all frames in the first trial. The reference image and each frame in the first trial were then contrast enhanced using a high-pass filter (Python scipy package, ndimage_gaussian_filter, sigma=50) to remove uneven background fluorescence. We then enhanced the edges of the high intensity areas by identifying the boundary as the difference between two low-pass filtered images (sigma=1 and 2, respectively) and adding 100 times of the boundary to the low-pass filtered image (sigma=2). Finally, we normalized the image by shifting its mean intensity value to zero and scaling the intensity of each pixel by the standard deviation across the whole frame. After contrast enhancement, we calculated the displacement of each frame by identifying the maximum cross-correlation between the reference image and the frame, and then shifted each frame accordingly. After motion correcting all frames in the first trial, we generated an updated reference image by averaging the pixel intensity across all frames in the now motion-corrected first trial. We then repeated the same motion correction procedure for all frames across all trials using the updated reference image.





Calcium imaging data analysis: regions of interest (ROI) segmentation, and fluorescence trace extraction

Neuron segmentation was performed with a customized deep learning network developed in Python with Tensorflow/Keras and based on U-net (Ronneberger et al., 2015). The training data were obtained from our previously published GCaMP6 datasets (hippocampus and striatum) and unpublished GCaMP6 datasets (striatum) (Mohammed et al., 2016; Shen et al., 2018). For each training dataset, we generated a projection image of the difference between maximum and minimum intensity of each pixel (max-min projection image), and manually curated a mask containing all identified neurons as ground truth, where neuron pixels were labeled as ones and background pixels as zeroes. The projected images and the corresponding ground truth masks were divided into small patches of 32x32 pixels, and each patch was normalized as following:

$$(I - I_{mean})/I_{std}$$

where I is the intensity of each pixel in the patch, I_{mean} and I_{std} are the averaged intensity and the standard deviation of the intensity across the patch, respectively. During training process, we randomly applied various image alterations (vertical and/or horizonal flip, rotation at 90, 180, and 270 degrees) to increase the robustness of the network.

To perform segmentation on the datasets for this study, we first generate the max-min projection images for each imaging session. We applied a moving window of 32x32 pixels with 50% overlap in both vertical and horizontal directions to the images to generate the inference data, resulting each individual pixels being inferred four times. Each 32x32 pixel patch was normalized as described above. For each pixel, the results from four inferences were averaged as a prediction score, and each pixel was classified as a neuron pixel if the score is greater than 0.5, or otherwise as a background pixel. Connected neuron pixels were then segmented and refined with watershed transformation to obtain the regions of interest corresponding to individual neurons.

After ROI segmentation, we extracted the fluorescence trace for each ROI from the motion corrected videos, and normalized each fluorescence trace as following:

$$(f - f_{mean})/f_{mean}$$

where the f is the observed fluorescence intensity at each time point of the trace, and f_{mean} is the averaged intensity during the ten seconds window before ultrasound onset.

Calcium imaging data analysis: identification of activated individual neurons

To identify whether a neuron is activated by ultrasound stimulation, we calculated, for each trial, the averaged GCaMP6 fluorescence during the baseline period (5 seconds before ultrasound onset) and during the response period (5 seconds after ultrasound onset). We then compared GCaMP6 intensities during the baseline period versus the response period across all 20 trials, using a Wilcoxon rank-sum test. A neuron was classified as activated if GCaMP6 intensity during the response period was significantly higher than that during the baseline period (Wilcoxon rank-sum, p < 0.05). To validate that the Wilcoxon rank-sum statistical method used to identify activated neurons was sufficiently powered, we applied a bootstrapping analysis by randomly selecting a time point (pseudo onset) during the 30-50 second period after ultrasound onset in a subset of recording sessions that contained 50 seconds of post stimulation period, which includes 14 hippocampus sessions with ultrasound stimulation and 7 with sham stimulation. After selecting the pseudo onset, we performed the same paired Wilcoxon rank-sum analysis as described above and repeated the process 20 times to obtain an expected number of activated neuron. This shuffled bootstrapping analysis returned a false positive rate of detecting activated neurons at $0.02 \pm 0.02\%$ for hippocampus session (mean \pm standard deviation, n=14 sessions) and 0.02 \pm 0.05% for sham sessions (mean \pm standard deviation, n=7 sessions), confirming that our statistical tests are sufficiently powered with a false positive rate of below 5% (p=0.05 threshold) as expected.

Calcium imaging data analysis: characterization of activation profiles in the hippocampus and the motor cortex

To estimate the latency of ultrasound evoked calcium responses across neuron populations in the hippocampus and the motor cortex, we first obtained the averaged the GCaMP6 fluorescence of each neuron





across all 20 trials, and then averaged across all neurons recorded in the same brain region. The onsets of ultrasound evoked population responses were defined as the time point where the average intensity of all activated neurons exceeds two standard deviations above the mean average intensity during the baseline period. We noted some tissue displacement in our motor cortex recordings upon ultrasound stimulation, which transiently reduced GCaMP6 signals as fluorescently labeled neurons moved out of the imaging focal plane. This transient reduction interferes with our onset latency estimation, and results in an under estimation of the exact time when GCaMP6f signals increased in the motor cortex.

To characterize the amplitude and the duration of ultrasound evoked responses across populations of individual neurons, we first averaged GCaMP6 fluorescence across all trails for each activated neuron. We then identified the peak of the evoked response as the time point when GCaMP6 fluorescence reached the maximum intensity during the response period. The peak amplitude of the evoked response was obtained by calculating the difference between the peak intensity and the minimum intensity between ultrasound onset and the peak. The duration of evoked responses was defined as the duration when GCaMP6 fluorescence remained above 50% of the peak amplitude.

Simulation of ultrasound intensity distribution in the brain

Intracranial ultrasound intensity distribution was modeled with k-Wave acoustic toolbox in MATLAB (Treeby and Cox, 2010) following the framework of Mueller et al. (Mueller et al., 2017). Representations of C57BL/6 skulls were formed from a three-dimensional atlas (Chan et al., 2007). To model our imaging experimental condition in the hippocampus, the skull was modified to include a craniotomy and an imaging window consisted of a stainless-steel imaging cannula with a glass coverslip positioned over the hippocampus. To model our imaging experimental condition in the motor cortex, the skull was modified to include a craniotomy, and a glass coverslip above the motor cortex. The mouse head model was coupled to the ultrasound source via water and considered immersed in air at 25°C and 50% humidity. For computational simplicity, soft tissue was considered homogeneous, and bone was considered homogeneous with bulk acoustic properties. Acoustic parameters for the various model components are listed below:

| Medium | c (m/s) | $\rho \left(kg/m^{3}\right)$ | $\alpha_0 (dB/MHz/cm)$ | у |
|-----------------|---------------------------|-------------------------------|--------------------------------|-----|
| Water | 1482 | 1000 | 0.0022 (Szabo, 1995) | 2 |
| Brain Tissue | 1562 (Szabo, 2014) | 1035 | 0.58 (Szabo, 2014) | 1.3 |
| Bone | 2850 (White et al., 2006) | 1732 (White et al., 2006) | 3.54 (Szabo, 2014) | 0.9 |
| Air | 343 | 1.20 (x100)* | 12 (Szabo, 1995) | 2 |
| Glass | 4540 | 2000 | 0.001737 (Kaye and Laby, 1995) | 2 |
| Stainless Steel | 5980 | 8000 | 0.00428 (Kaye and Laby, 1995) | 2 |

^{*} Density of air was artificially raised to prevent computational errors due to impedance mismatch, as recommended by k-Wave. The reflection coefficient remained close to one.

The computational grid for linear simulations had a discretization of 0.12 mm, corresponding to 28 points per wavelength in water. Time steps were determined with k-Wave's built-in function to ensure simulation stability. The single-element unfocused ultrasound transducer was modeled with a 12.36 mm diameter to fit on the computational grid. The transducer emitted ultrasound as those used in the experiment (75-cycle ultrasound burst with center frequency of 350 kHz and pressure peak amplitude of 0.44 MPa) for all simulations. The maximum and root mean square (RMS) instantaneous pressure at the motor cortex and the hippocampus was recorded, and the maximum instantaneous pressures were used to produce pressure distribution maps.